



## Scientific-Research Article

# Numerical Simulation of Combustion to Identify and Eliminate Power Reduction Problem of a Gas Turbine Engine

Hamed Arhami<sup>1</sup>, Mohammad Mazidi Sharfabadi<sup>2\*</sup>

1-Islamic Azad University, Research and Sciences Branch, Tehran, Iran

2- Development and Optimization of Energy Technologies Division, Research Institute of Petroleum Industry (RIPI), Tehran, Iran

## ABSTRACT

**Keywords:** numerical simulation, three-dimensional turbulent flow, combustion chamber, engine test cell, defective engine

*In this research, a three-dimensional numerical simulation of the combustion inside the combustion chamber of a typical turboprop engine has been done, and the velocity, pressure, temperature fields as well as the temperature distribution within the wall of the combustion liner have been obtained. The complex geometry of this combustion liner was generated according to the available technical drawings. The computational domain was meshed, and the non-premixed combustion model and the K- $\omega$  turbulent model were used to simulate the combustion and the turbulent flow, respectively. With the help of this simulation, the inefficiencies of combustion liners were recognized and by improving them, the problem of reducing the power of several gas turbine engines tested in an industrial test cell was solved. The simulation results of the combustion liner show that the existence of the weld line created in the repair process near its outlet has increased the pressure drop by 25% compared to the typical one, and the effective cross-sectional area of the fluid flow has decreased by 11%. Furthermore, the results show that the velocity profile and the pattern of the outlet temperature of the repaired combustion liner are different from its typical one.*

## Introduction

With the advancement of computer science, it is possible to simulate very complex problems. One of the most complicated concerns for numerical simulation is combustion. Laboratory investigations of this phenomenon, especially in gas turbines, are very expensive and time-consuming and do not

show details. The high-accuracy numerical investigations which match the laboratory results are cheap and fast. Nowadays, the numerical investigation of the combustion phenomenon plays a very important role in the most advanced industries of the world.

Bouchard et al. [1] experimentally investigated the combustion chamber of a gas turbine engine and

1 PhD student

2 Assistant Professor (Corresponding Author) **Email:** hamedarhami66@gmail.com

stated that the improper temperature distribution at the outlet causes inappropriate mixing of the dilution air with the combustion flow. Babu et al. [2] worked on improving the temperature distribution at the exit of the air gas turbine combustor. They obtained the best exit temperature for three different designs. Gouws [3] analyzed the flow inside the combustion chamber of a gas turbine engine by using one-dimensional code, and three-dimensional numerical analysis and compared them with experimental results. He investigated the effect of changing the swirler in several different designs on the outlet temperature distribution. The effect of different fuels on the chamber parameters such as output temperature, wall temperature, combustion efficiency, NO<sub>x</sub>, and soot generation of a gas turbine engine has been investigated [4-7]. Skidmore et al. [8,9] have also investigated the smoke generation of the combustion chamber in a laboratory, and they [10] have also investigated the flow rate passing through the cooling holes of the chamber. Wang et al. [11] have studied the use of thermal barrier coatings instead of improving the cooling of the chamber. Guy et al. [12] designed and improved a gas turbine combustion chamber by simulating several geometric models of the chamber and choosing the best model in terms of carbon monoxide emission reduction. In another research [13], the characteristics of fuel spraying have been investigated in a laboratory. Three-dimensional numerical simulation of the combustion chamber of a gas turbine engine has been carried out by Enagi et al. [14] and the results have been compared with reference [4]. Also, by dividing the chamber into smaller segments and using a one-dimensional network solution, the main parameters of the analysis have been investigated.

In previous analyses, comprehensive data about the phenomena inside the combustion chamber was not available, and it was not possible to study the effects of each part of the combustion chamber on the combustion process. In this research, the simulation of combustion inside the combustion chamber of a gas turbine engine has been studied. The combustion liner geometry was generated according to the technical drawings and the simulation of the turbulent flow and combustion inside it was done numerically and three-dimensionally. To simulate the combustion, the non-premixed combustion model and the k- $\omega$  model were used to simulate the turbulent flow. This simulation deals with how the combustion phenomenon occurs, how the gas temperature is distributed inside, the outlet, and also

the wall of the combustion chamber. This simulation gives suitable ideas to discover the weak points of the combustion liner and also to provide solutions to eliminate these weaknesses, and its results have been used to discover the defects of gas turbine engines.

### The turboprop engine and its combustion chamber

The engine studied in this research is a single-spool turboprop. This engine has a 14-stage axial flow compressor that is driven by a 4-stage turbine. The gearbox of the engine with a constant rotation speed of 13820 rpm gives power equivalent to 4910 hp. In the take-off regime, the mass flow rate of the air entering the engine is 14.154 kg/s and its air-to-fuel ratio is 0.02. Also, the aero-derivative version of this engine is used for all kinds of industrial and marine power generation purposes. The can-annular combustion chamber of the turboprop engine includes 6 combustion liners with a length of 0.548 m. Figure 1 shows the schematic view of the turboprop engine combustion chamber.

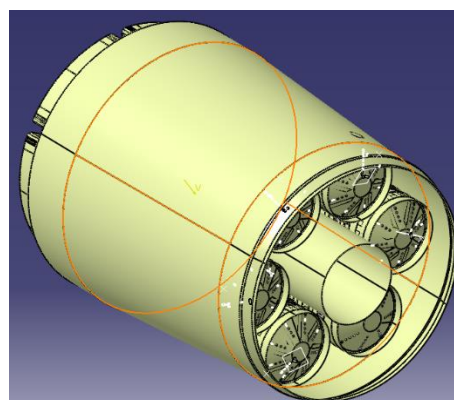
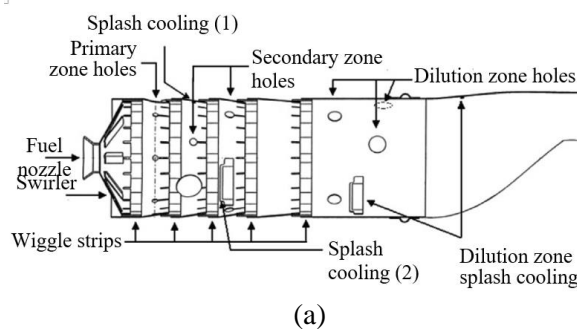
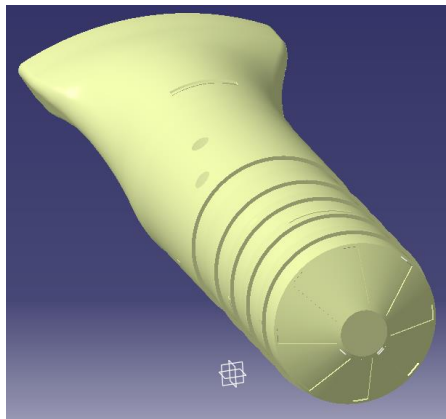


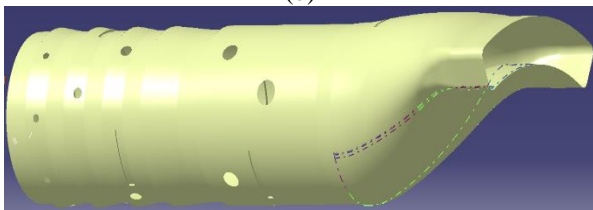
Figure 1. Schematic view of the combustion chamber

This chamber includes primary, secondary, and dilution regions. As shown in Figure 2, the primary region consists of one row and the secondary and dilution regions consist of two rows of air inlet holes. 8 rows of splash cooling strips are installed on the dome of the combustion chamber for making rotation in the entering air as well as cooling of this part of the chamber. Also, film cooling of the wall is possible through 8 rows of wiggle strips placed along the wall of the combustion liner and several other splash cooling systems.





(b)

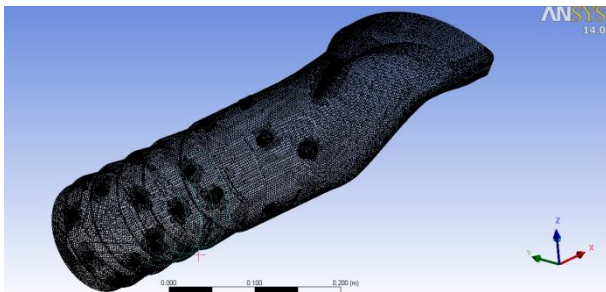


(c)

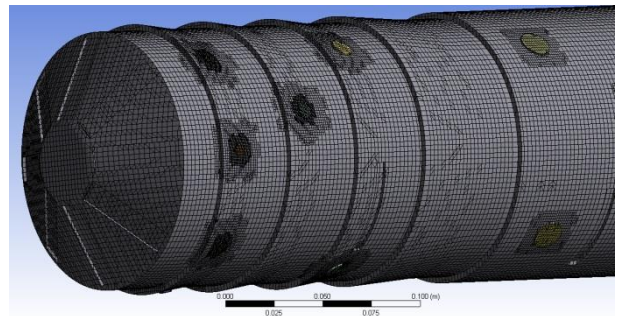
**Figure 2.** Schematic view of the combustion liner (a) film cooling and dilution holes (b) front view and fuel injection site (c) side view and combustion liner outlet

### Geometry modeling and meshing

The first step in the simulation of the combustion chamber is its geometrical design. The combustion chamber of the engine has many geometrical complexities, so its design requires a lot of precision. Catia software was used to design the geometric model of the engine combustion chamber. Due to the symmetry of 6 combustion liners, only one of these liners can be simulated for thermal and hydrodynamical analysis. After the geometrical modeling of the combustion liner, it is time to mesh the computational domain. Figure 3 shows the different grid views of the computational domain.



(a)



(b)

**Figure 3.** Computational domain meshing (a) whole combustion liner (b) close-up view (red circle)

The independence of the solution from the size of the control volumes is checked. Figure 4 shows the independence of the solution from the grid size for the mean temperature of the combustion liner outlet. It can be seen that for 1,000,000 meshes, the desired quantity becomes constant. Therefore, the results presented in the following sections are obtained based on the number of meshes.

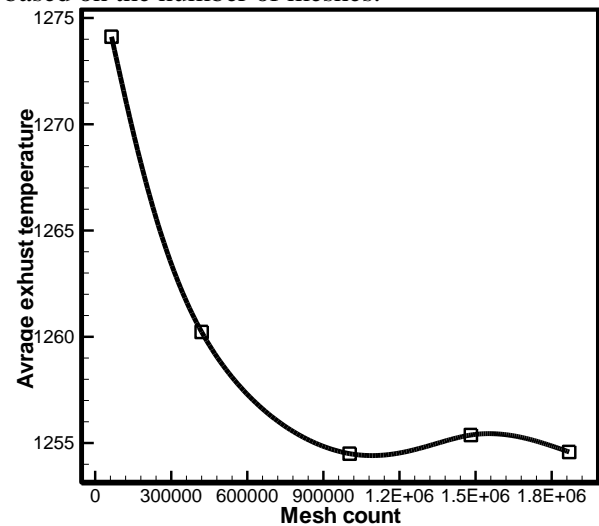


**Figure 4.** The independence of the solution from the number of meshes

### Governing equations and boundary conditions

In this research, the Mach number inside the combustion chamber is less than 0.3, so it can be assumed that the flow is incompressible. The equation of conservation of mass is one of the most important equations for analyzing the reaction of species. This equation is defined as follows:

$$\frac{\partial \rho}{\partial t} + \nabla \cdot \rho u = 0 \quad (1)$$

The conservation of momentum equation can be expressed as the following equation:

$$\rho \left( \frac{\partial u}{\partial t} + \nabla u \cdot u \right) = -\nabla p + \rho g + \nabla \cdot \mu \nabla (u + u^T) + \sigma \kappa \delta(\varphi) \nabla \varphi \quad (2)$$

Also, to simulate combustion, it is necessary to apply the conservation of energy equation:

$$\begin{aligned} \frac{\partial}{\partial t}(\rho E) + \nabla \cdot (\vec{v}(\rho E + p)) \\ = \nabla \cdot \left( k_{eff} \nabla T \right. \\ \left. - \sum_j h_j \vec{j}_j + (\bar{\tau}_{eff} \cdot \vec{v}) + Sh \right) \end{aligned} \quad (3)$$

where:

$$E = h - \frac{p}{\rho} + \frac{u_i^2}{2} \quad (4)$$

For premixed combustion, equation (3) is rewritten as follows:

$$\frac{\partial}{\partial t}(\rho E) + \nabla \cdot (\rho \vec{v} H) = \nabla \cdot \left( \frac{k_t}{c_p} \nabla H \right) + S \quad (5)$$

where H is obtained by equation (6):

$$H = \sum_j Y_j H_j \quad (6)$$

$$H_j = \int_{T_{ref,j}}^T C_{p,j} dT + h_j^0(T_{ref,j}) \quad (7)$$

### Turbulence modeling

In this study, the standard k- $\omega$  model is used to simulate the turbulent flow. Considering the low flow velocity in most areas and the effect of the combustion liner walls, this model showed a very good solution in convergence. In this model, turbulence kinetic energy (k) and specific dissipation rate ( $\omega$ ) are obtained from the following equations:

$$\frac{\partial}{\partial t}(\rho k) + \frac{\partial}{\partial x_i}(\rho k u_i) = \frac{\partial}{\partial x_j} \left( \Gamma_k \frac{\partial k}{\partial x_j} \right) + G_k - Y_k \quad (8)$$

$$\frac{\partial}{\partial t}(\rho \omega) + \frac{\partial}{\partial x_i}(\rho \omega u_i) = \frac{\partial}{\partial x_j} \left( \Gamma_\omega \frac{\partial \omega}{\partial x_j} \right) + G_\omega - Y_\omega \quad (9)$$

In these equations, the turbulence kinetic energy,  $G_k$ , is caused due to the average velocity gradients.  $G_\omega$  represents the generation of  $\omega$ .  $\Gamma_k$  and  $\Gamma_\omega$  are the effective permeability k and  $\omega$  due to turbulence.  $Y_k$  and  $Y_\omega$  are user-defined source terms.

### Numerical simulation method

In this study, a non-premixed combustion model was used to simulate combustion. This model includes solving energy equations for one or two conservative scalars (mixed fraction). The equations are not solved for individual species. Instead, species concentrations are derived from predicted mixture fraction fields. Thermochemical calculations are preprocessed and then indexed in Ansys-Fluent for searching. The interaction of

turbulence and chemistry is calculated for the assumed probability density function. In this equation, the reaction of kerosene with air is not directly converted into  $\text{CO}_2$  and  $\text{H}_2\text{O}$ , but it is first broken into the species presented in Table 1 (similar to what happens in reality). The probability function table of kerosene fuel density is shown in Table 1.

**Table 1.** Species involved in intermediate reactions

No.	species	No.	species
1	NO	9	HNO
2	NO <sub>2</sub>	10	CN
3	N <sub>2</sub> O	11	H <sub>2</sub> CN
4	H <sub>2</sub> O (l)	12	HCNN
5	N	13	HCNO
6	NH	14	HOCN
7	NH <sub>2</sub>	15	HNCO
8	NH <sub>3</sub>		

### Boundary conditions

#### Fuel injection

In this research, fuel injection is considered as a cone, the specifications of which are given in Table 2.

**Table 2.** Characteristics of the simulated fuel injector [3]

Parameter	Value
Velocity (m/s)	30
Mass flow rate (kg/s)	0.04742
Cone half-angle (deg)	55
Temperature (K)	300
Radius (mm)	0.3937008
Rotation ratio	0.5
Number of particle diameters	12
Particle diameter distribution method	Rosin-Rammler
Minimum particle diameter (mm)	0.0002704724
Maximum particle diameter (mm)	0.009437008
The average diameter of atoms (mm)	0.003785827
Evaporating substance	C <sub>12</sub> H <sub>23</sub>

### The flow rate of air inlet holes

The airflow rate through different types of inlet holes is given in Table 3. These data are published in reference [3] and they are used as input to the problem.

**Table 3.** Boundary conditions of air inlet holes [3]

Fluent Inlet designation	Flow splits [%]	Flow splits [kg/s] 2.37642	Splits to individual holes [kg/s]
Injector	0.7448178	0.0177	0.0177
shell swirl 1			0.08551
shell swirl 2			0.05938
shell swirl 1+2	6.0969862	0.14489	
wigg 1 bottom			0.18428
wigg 1 top			0.18428
wigg 1 total	15.509043	0.36856	
shell2 hole 1			0.016245714
shell2 hole 2			0.016245714
shell2 hole 3			0.016245714
shell2 hole 4			0.016245714
shell2 hole 5			0.016245714
shell2 hole 6			0.016245714
shell2 hole 7			0.016245714
shell 2 hole total	4.7853494	0.11372	
wigg 2 bottom			0.12605
wigg 2 top			0.12604
wigg 2 total	10.607973	0.25209	
shell3 splash	0.1880981	0.00447	
shell 3 hole 1			0.00447
shell 3 hole 2			0.027606667
shell 3 hole 3			0.027606667
shell 3 hole total	3.4850742	0.08282	
wigg 3 bottom			0.13055
wigg 3 top			0.13055
wigg 3 total	10.987115	0.2611	
shell4 hole 1			0.0389175
shell4 hole 2			0.0389175
shell4 hole 3			0.0389175
shell4 hole 4			0.0389175
shell 4 hole total	6.5506097	0.15567	
shell 4 splash 1			0.00977
shell 4 splash 2			0.00977
shell 4 splash total	0.8222452	0.01954	
wigg 4 bottom			0.1131

**CLAD1 software**

CLAD1 is a user-friendly software package with a graphical user interface that was implemented and developed in MATLAB software. As the aim of this software, the flow and pressure and temperature distribution along the combustion chamber can be estimated.

Flow splitting and pressure drop prediction are obtained by the flow split function, and the gas temperature at each node along the axis of the combustion liner is calculated by the combustion function. Combustion efficiency can be taken into account during these calculations. The elements' function calculates the properties at each node, which are used in the heat transfer function. The heat transfer function predicts the heat transfer along the combustion liner at each node. Figure 5 shows the sequence of calculations in CLAD1 software.

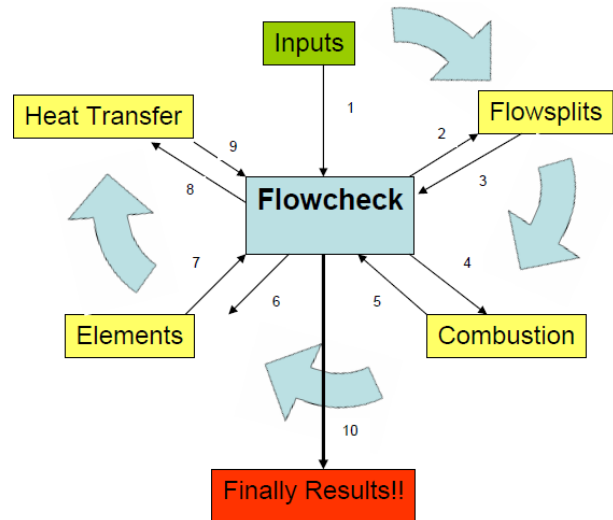
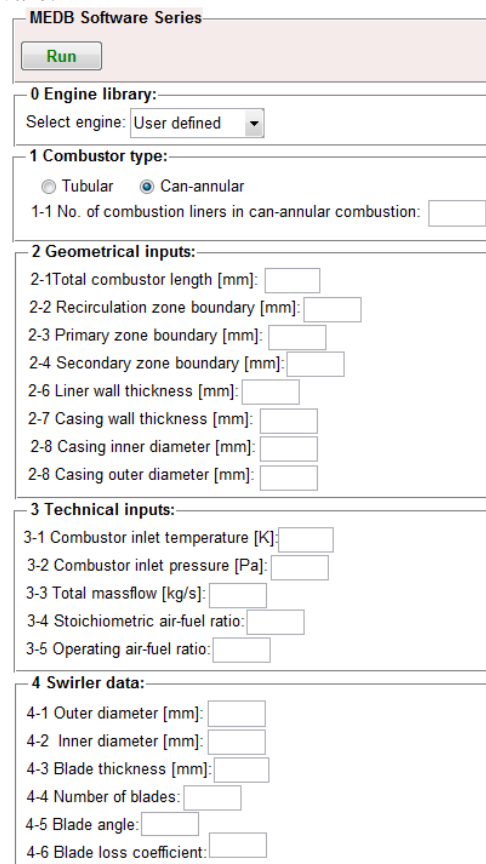


**Figure 5.** The sequence of calculations in CLAD1 software [3]

Figure 6 shows the graphic user interface of CLAD1 software. Film cooling rate and the amount of pollution emission can be simulated as well. The combustion efficiency, liner pressure drop, and CO, UHC, and NOx pollutants emission (in grams per kilogram of fuel) can also be calculated in the software.



**5 Hole layout:**

5-1 No. of hole sets:

	Hole type	No. of holes	Hole diameter [mm]	Hole set pos:
1	0	0	0	0
2	0	0	0	0
3	0	0	0	0
4	0	0	0	0

**Notes:**  
 - Not DIAMETER of Wiggle strip, but slot width.  
 - If value is 0, discharge coefficient will be calculated.  
 (Set only 0 for Plain and Plunged holes)

**6 Zones layout:**

6-1 Number of combustion zones:

6-2 Number of nodes in each zone:

6-3 Fraction of mass flow into each zone:

	Recirculation	Primary	Secondary	Dilution
1				
2				
3				

**7 Heat transfer:**

7-1 Ambient temperature [degC]:

7-2 Liner wall conductivity [W/m K]:

7-3 Casing wall conductivity [W/m K]:

7-4 Radiation model:

7-5 Liner inner emissivity:

7-6 Liner outer emissivity:

7-7 Casing inner emissivity:

7-8 Casing outer emissivity:

7-9 Out-side convection:

Casing out-side heat transfer coefficient [W/m<sup>2</sup> K]:

Out-side radiation

Film cooling

Combustion efficiency calculation

7-10 Nox emission model:

**8 Results:**

Write data file

Select data:

8-1 Pressure loss [Pa]:   [%]

8-2 Pattern factor \*10<sup>6</sup>:

8-3 Combustion efficiency [%]:

8-4 Emission indices [g/kg fuel]:  
 CO:  CO<sub>2</sub>:  NOx:

8-5 Emission combustion efficiency [%]:

Figure 6. The graphical user interface of CLAD1 software

### Engine test cell

The turboprop engine is tested in an engine test cell, after being installed on the test bed and connected to

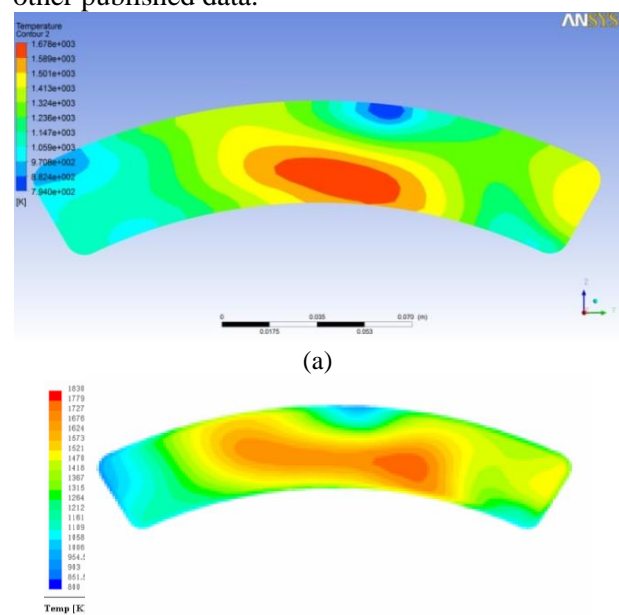
the dyno. The engine is evaluated in four working regimes defined based on the exit temperature of the combustion chamber. The task of the dyno is to keep the rotational speed of the engine constant after reaching 100% during the test. The dyno does this by adjusting the mass flow rate of the water passing through it and as a result absorbing the power of the engine to keep the engine speed constant. The performance parameters for each of the working regimes are recorded in the run sheet for evaluation.

### Results and discussion

The results of the current research presented in the following section have been used to solve the problem of efficiency reduction of several under-studied engines.

### Validation of simulation results

The main purpose of the combustion chamber is to create hot gas with a predefined and uniform temperature distribution to enter the turbine. The more uniform the temperature distribution is, the less damage the turbine parts get. Each kind of combustion chamber has its outlet temperature distribution, so it can be used as a basis for comparing and validating research results. The comparison of the results of the present numerical study with the other numerical work results [3] and experimental data [3] is given in Figures 7 and 8. Comparing the figures shows that the results of the present research have a very close pattern to the other published data.



(a)

(b)

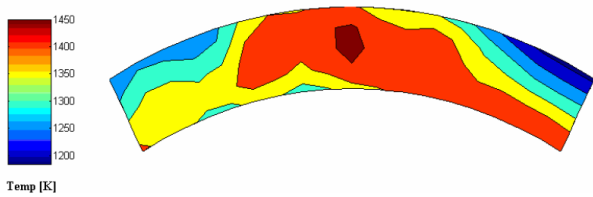


**Figure 7.** Combustion liner outlet temperature distribution (a) Current numerical research (b) Numerical simulation [3] (c) Experimental results [3]

The radial temperature distribution of the gas at the outlet of the combustion liner is shown in Figure 8. By comparing the results of this research and reference [3], it can be seen that the output temperature distribution of both numerical solutions was very close to each other and even the numerical solution of this research is closer to the test bed results. In this figure, it can be seen that the maximum temperature occurs near the bottom wall.

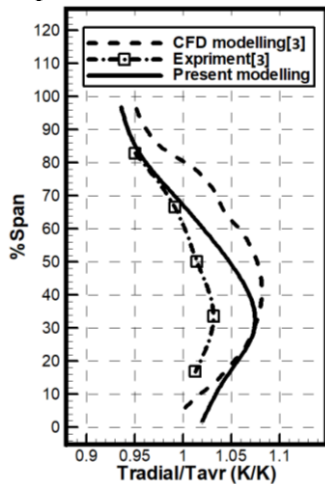


**Figure 8.** Radial temperature distribution at the outlet of the combustion liner

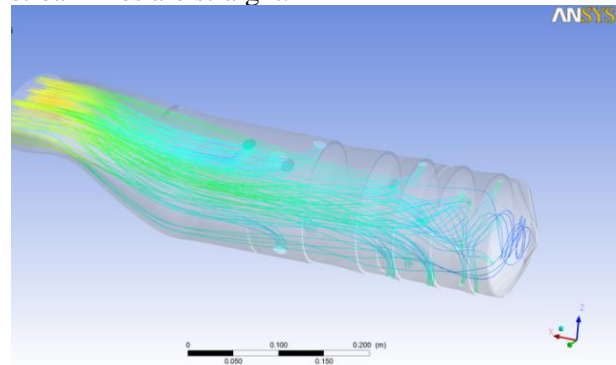
The comparison of the average temperature output of the present numerical simulation with CLAD1 software results and experimental results is shown in Table 4. It can be seen that the results are very close to each other and have a good overlap. The reason for the lower average temperature of the combustion chamber outlet in the numerical analysis compared to the actual temperature is the lower heating value of kerosene fuel compared to JP-4 used in the experimental study.

Table 4. Comparison of the average outlet temperature obtained from different methods

Method	Average outlet temperature (K)
CLAD1 one-dimensional software	1255
3D numerical analysis	1277
Experimental results [3]	1350

### Streamlines through film cooling and dilution holes

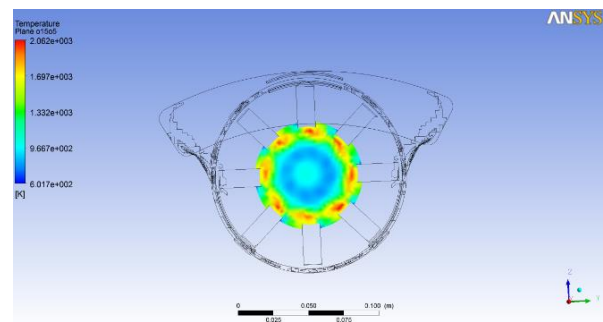
Figure 9 shows the flow path of the fluid through some holes in the combustion liner. It can be seen that except in the primary and secondary zones of the combustion liner where the flow is rotational, the streamlines are straight.



**Figure 9.** Streamlines through film cooling and dilution holes

### Temperature distribution in different sections of the combustion liner

The fluid temperature contour at different sections of the combustion liner is shown in Figure 10. These figures clearly show the location of the flame formation. At the beginning of the combustion liner, vortices are formed near the wall, these vortices carry fuel sprayed upstream. The purpose of the holes in the primary zone is to inject air for burning fuel. Therefore, the temperature in these areas is high. The flame propagates along the combustion liner. The cold streaks seen in the middle of the hot stream in Figure 10 (c) are due to the injection of air from the holes in the wall of the combustion liner



(a)

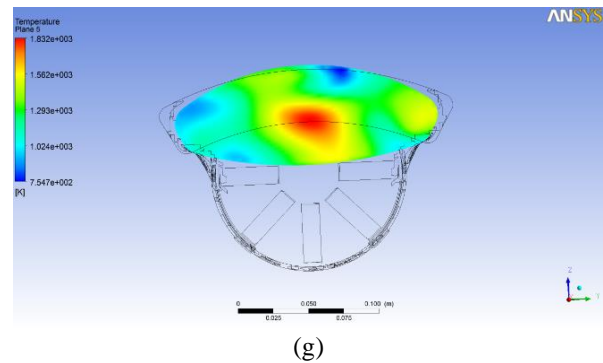
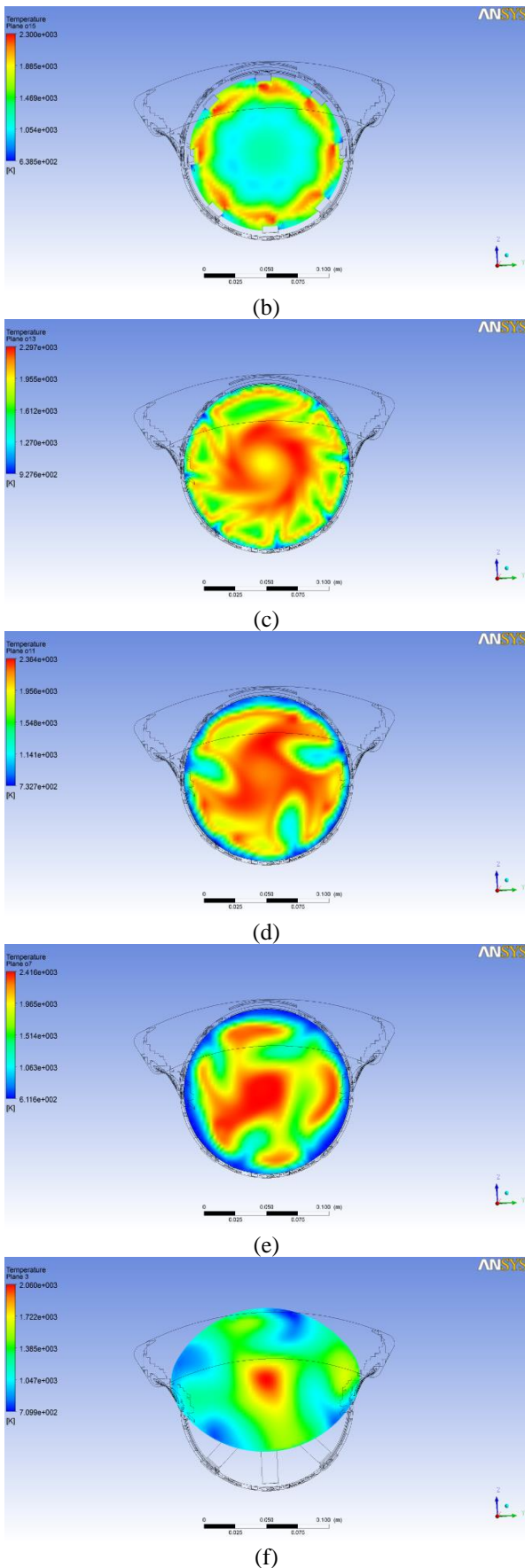


**Figure 10.** The average temperature of the fluid in sections with distance (a) 0.41 (b) 0.91 (c) 2.91 (d) 4.91 (e) 8.91 (f) 18.91 (g) 20.91 inches from the dome of the combustion liner

The average temperature of the fluid at different points along the axis of the combustion liner for three different numerical solutions (reference [3]), the one-dimensional solution of the CLAD1 software, and the results of the present research are illustrated in Figure 11. It can be seen that the curve obtained from the current numerical solution in most of the points along the axis of the combustion chamber is close to the numerical solution presented in reference [3], while the fluid temperature at the combustion liner exit is closer to the results of CLAD1 software.

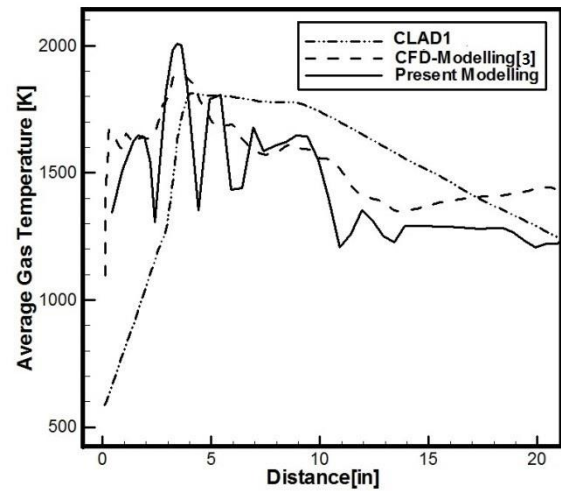


**Figure 11.** Comparison of the average temperature of the fluid along the combustion liner axis

In Figure 12, the average temperature of the combustion liner wall along the axis of the combustion liner for three numerical solutions (reference [3]), network solution and the results of the present research are presented. It should be mentioned that to calculate the average temperature of the wall or fluid along the combustion liner axis, planes have been passed at different sections along the combustion liner axis and the average

temperature of the wall at each section has been calculated. It can be seen that the results of this research are close to the numerical solution published in reference [3] for most of the points along the combustion liner. Five temperature jumps along the combustion liner are due to the presence of film cooling and dilution holes. The reason for the higher temperature jump in the current work results is the simplifications made in the simulation of these holes. In the experiment, a new number of sensors are installed in certain places, and sometimes geometric limitations prevent the sensor from being installed in the cooling and dilution holes. Therefore, a curve is fitted for the temperature distribution. On the other hand, in the numerical method, the temperature is estimated for all points along the combustion liner wall.

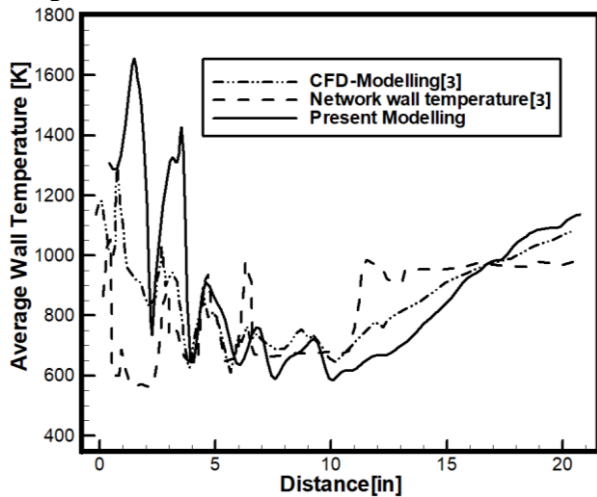


**Figure 12.** The average temperature of the wall along the combustion liner axis

In the last half of the combustion liner the wall temperature increases. The reason for this is the lack of proper film cooling in this part, especially near the outlet. Reducing cross-sectional area in this region causes the fluid to accelerate and increase the heat transfer coefficient and the heat transfer rate to the wall.

Figure 13 shows the temperature distribution in the middle plane of the combustion liner. It can be seen that the temperature is low in the areas near the walls, but in parts of the combustion liner where film cooling is not performed well, the metal surface meets higher temperatures.

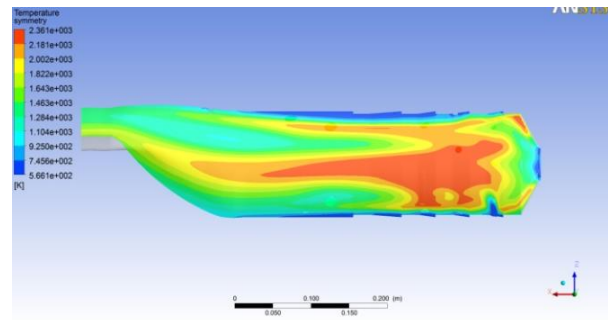


**Figure 13.** The fluid temperature in the middle plane of the combustion liner

### Examination of the condemned combustion liners

Figures 14 and 15 show that the swirlers and the fish mouth part of the condemned combustion liners suffer from buckling, cracks, and hot spots due to the performance of the combustion chamber.

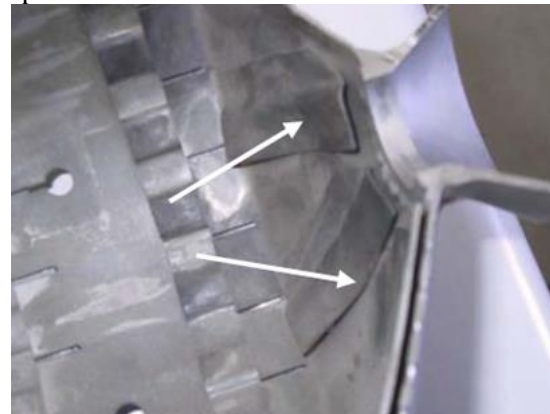


**Figure 14.** Distortion of swirler vanes in a condemned combustion liner



**Figure 15.** Cracks in the outlet part of a condemned combustion liner

The simulation results (Figure 10 (a) and 16) show that the swirler vanes (Figure 16) and the lower wall of the fish mouth part near the exit (Figure 10 (a)) of the combustion liner meet high temperatures. It is due to the defects in the design of this type of combustion liner. They suffer from such improper film cooling as shown in Figures 14 and 15.

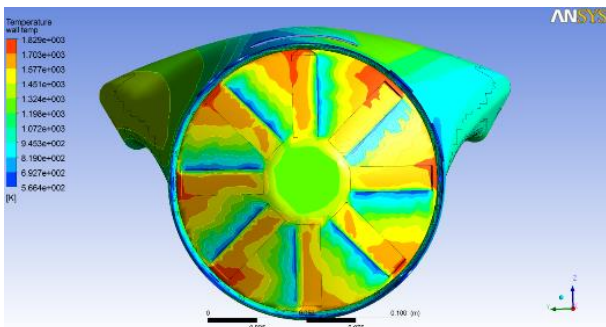


Figure 16. Combustion liner dome temperature contour

### Investigating power reduction of several engines in the test cell

Several engines were tested in the test cell experienced power reduction problems. After the investigation of combustion chambers, two suspicious cases were encountered:

- 1- A repairing welding line on the lower wall of the fish mouth area, near the exit of the combustion liner, exists. According to the engine technical manual for maintenance, any obstacles in this area may cause a problem in combustion liner performance.
- 2- The opening of the combustion liner outlet is wider than the limit published in the technical manual of the engine.

In the engine technical manual, it is emphasized on maintaining the dimensions of the exit and the absence of any obstacles in this area. There is no such emphasis on other parts of the combustion chamber. The complex geometry of the fish mouth section that narrows the passage of hot gases and the connection of this part to the turbine nozzle guide vanes have increased the dimensional sensitivity of this area.

### The formation of a welding line in the repairing process of the combustion liner

In the repairing process of some combustion liners, a welding line is created on the lower wall of the exit passage, whose schematic is shown in Figure 17. The height of this welding line is about 1.5 mm, which is equivalent to about 7% of the height of the outlet opening. For simulating the combustion liner with defects, a semi-cylindrical obstacle with a height of 1.5 mm, similar to a welding line is added to the geometry of the combustion liner in that area and a new grid was created for it. Then, the simulation process was repeated in the same way as before.

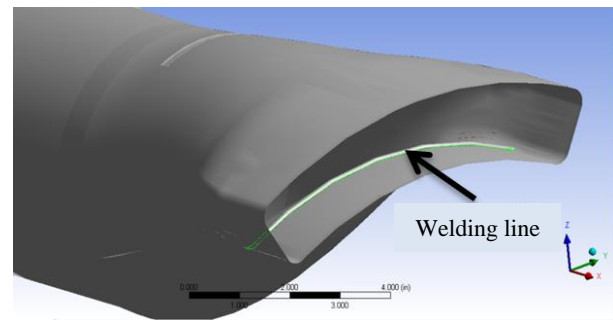


Figure 17. Schematic of the welding line at the exit of the gas turbine combustion liner

Figures 18 and 19 show the temperature distribution of the middle plane near the exit of the combustion liner for two combustion liners with and without the weld line. The results of numerical simulations show that the repaired combustion liner has 25% more pressure drop than the typical combustion liner, and the amount of the effective cross-sectional area of the fluid flow in the repaired type is reduced by 11%. Also, the velocity and temperature profile patterns at the outlet of the repaired combustion liner are different from the typical one. The simulation results of this research for the geometric defects are consistent with the strong emphasis on the sensitivity of the dimensions of the combustion liner exit presented in the engine technical manual. Based on the above simulation results, after removing this defect, the engine was tested again in the test cell and it was observed that the problem of reducing the engine power had been solved.

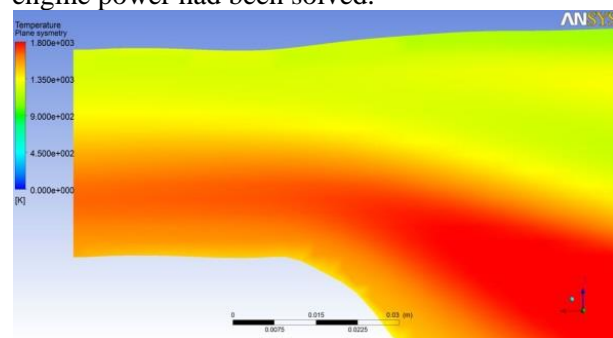


Figure 18. Temperature distribution near the exit of a typical combustion liner

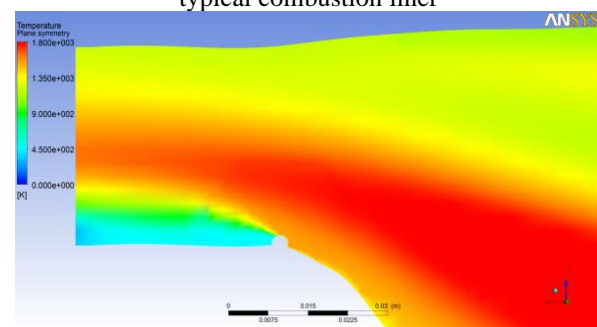
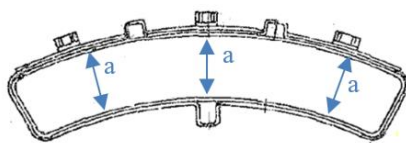


Figure 19. Temperature distribution near the outlet of a repaired combustion liner with a weld line height of 1.5 mm

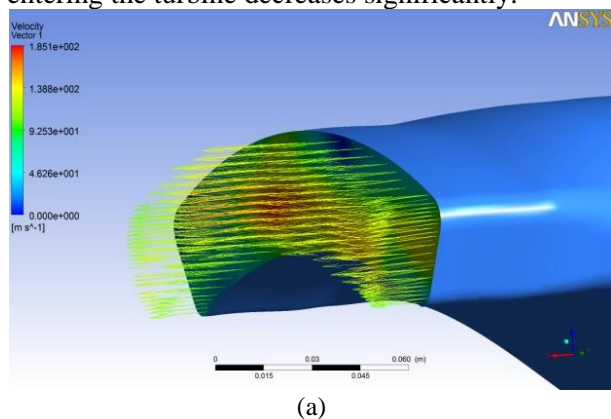
### Excessive area of the combustion liner outlet

Another problem of some combustion liners is the deviation from the allowed limits of the outlet cross-section dimensions (Figure 20). It seems to be not important before the investigations are carried out in this research. The outlet of the combustion liner is placed on the first stage of the turbine vanes. Considering that the pressure outside the combustion liner is higher than inside if the dimensions of the outlet opening of the combustion liner are greater than the permissible dimensions, the airflow from outside to the inside of the combustion liner is created in that area and disturbs the temperature distribution of the outlet of the combustion liner. At this stage, to simulate this defect, the outlet opening was considered to be 3 mm wider, and the results of the simulation of this issue are presented below.

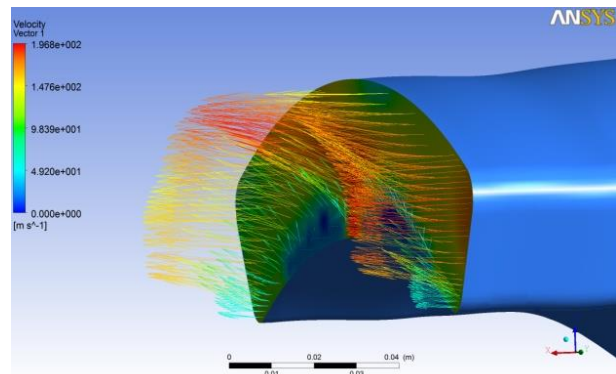


**Figure 20.** Height of the outlet opening of the combustion liner

Figure 21 shows the streamlines through the combustion liner outlet in the cases where the outlet dimensions are within the permitted range (Figure 21 (a)) and larger than the permitted dimensions (Figure 21(b)). It can be seen that if the cross-sectional area is larger than the permissible dimensions, the streamlines become irregular and this causes the velocity triangle at the turbine inlet to change improperly. Furthermore, the thermal analysis shows that the temperature of the fluid entering the turbine decreases significantly.



(a)



(b)

**Figure 21.** Streamlines through the outlet of (a) typical (b) defective combustion liner

After the geometric modifications, the modified combustion liners were installed on the engine and it was tested in the test cell and met the test criteria. With this modification, the power reduction problem of several other engines was also solved. Based on the results of the simulation and performance test of the engine, corrections were made in the repair technical manuals of the combustion liner. It was emphasized to check and maintain the exact geometrical dimensions of the combustion liner exit.

### Conclusion

In this research, the results of the combustion three-dimensional numerical simulation of the engine combustion liner of a gas turbine engine have been presented. The comparison of the results of the present research with a similar numerical analysis shows that the results of this work are in good agreement with the experimental results. The defect of this type of combustion chamber is the lack of sufficient cooling in the area of the primary and transition duct passage, which must be overcome.

The simulation results of the combustion liner defects show that the combustion liners with a weld line near the outlet have a 25% higher pressure drop than the typical combustion liner, and the effective cross-sectional area of the fluid flow is reduced by 11%. Also, the velocity profile and the outlet temperature distribution of the repaired combustion liner are different from its typical type.

Another defect of some of the combustion liners is the excessive cross-section area of the outlet. It can be seen that in the case where the cross-section area is larger than the allowed dimensions, the streamlines become irregular and this causes the velocity triangle at the turbine inlet to change improperly. Also, the thermal analysis shows that

the temperature of the fluid entering the turbine decreases significantly.

After the geometric modifications, modified combustion liners were installed on the engines and tested in the test cell. All the engines were tested successfully and the power reduction problem was solved.

## References

- [1] D. Bouchard and G. Pucherand and W. D. E. Allan, "Can annular combustion chamber surface temperature measurements and damage signatures at operationally representative conditions", *ASME Turbo Expo*, GT2011-46639, pp. 2027-2035, 2011.
- [2] D. A. babu and K. K. Arun and R Anandanarayanan, "Optimization of pattern factor of the annular gas turbine combustor for better turbine life", *IOSR Journal of Mechanical and Civil Engineering (IOSR-JMCE)*, pp. 30-35, 2009.
- [3] J. J. Gouws, "Combining a one-dimensional empirical and network solver with computational fluid dynamics to investigate possible modification to a commercial gas turbine combustor", Master of Engineering Thesis, *Faculty of Mechanical/Aeronautical Engineering University of Pretoria*, 2007.
- [4] K. N. Rizk and V.L. Oechsle and P.T. Ross and H.C. Mongia, "High density fuel effects", IN 46206-0420, *Allison Gas Turbine Division, General Motors Corporation*, 1988.
- [5] D. Cerinsk and M. Vujanovic and Z. Petranovic and J. Baleta and N. Samec and M. Hribersek, "Numerical analysis of fuel injection configuration on nitrogen oxides formation in a jet engine combustion chamber", *Energy Conversion and Management*, vol. 220, 112862, 2020.
- [6] S. Maspanov and I. Bogov and A. Smirnov and S. Martynenko and V. Sukhanov, "Analysis of gas-turbine type GT-009 M low-toxic combustion chamber with impact cooling of the burner pipe based on combustion of preliminarily prepared depleted air–fuel mixture", *Energies*, vol. 15, No. 3, 707, 2022.
- [7] L. Jiang and A. Corber, "Assessment of combustor working environments", *International Journal of Aerospace Engineering*, 217463, 2012.
- [8] F. W. Skidmore and D. R. Hun and P. N. Doogood, "The reduction of smoke emissions from allison engine", *Defence Science and Technology Organization Aeronautical Research Lab, Melbourne, Victoria*, 1990.
- [9] F. W. Skidmore, "Smoke emissions test on series ii and iii allison turboprop engines", *Defence Science and Technology Organization Aeronautical Research Lab. Melbourne, Victoria*, 1986.
- [10] F. W. Skidmore and W. H. Schofield, "The variation in airflow coefficient for allison combustor liners (U)", *Defence Science and Technology Organization Aeronautical Research Lab. Melbourne, Victoria*. 1987.
- [11] J. Wang and Z. Li and F. Li, "Stress and displacement distribution of the thermal barrier coatings in the turbine engine combustion chamber", *Coatings*, vol. 10, no. 9, 842, 2020.
- [12] S. R. D. Guy and W. D. E Allan and M. LaViolette and P.R. Underhill, "Optical patterning of gas turbine fuel spray during simulated engine operating conditions", *Proceedings of ASME Turbo Expo*, GT2009-59011, pp. 1-10, 2009.
- [13] K. N. Rizk and H. C Mongia, "Three-dimensional combustor performance validation with high density fuels", *Propulsion*, vol. 6, no.5, pp. 660-667, 1990.
- [14] I. I. Enagi and K. A. Al-attab and Z. A. Zainal, "Combustion chamber design and performance for micro gas turbine application", *Fuel Processing Technology*, vol. 166, pp. 258-268, 2017.

---

## COPYRIGHTS

©2022 by the authors. Published by Iranian Aerospace Society This article is an open access article distributed under the terms and conditions of the Creative Commons Attribution 4.0 International (CC BY 4.0) (<https://creativecommons.org/licenses/by/4.0/>).

---

